

Stability of Polymer:PCBM Thin Films under Competitive Illumination and Thermal Stress

Sebastian Pont, Fabrizia Foglia, Anthony M. Higgins, James R. Durrant, and João T. Cabral*

The combined effects of illumination and thermal annealing on the morphological stability and photodimerization in polymer/fullerene thin films are examined. While illumination is known to cause fullerene dimerization and thermal stress their dedimerization, the operation of solar cells involves exposure to both. The competitive outcome of these factors with blends of phenyl-C61-butyric acid methyl ester (PCBM) and polystyrene (PS), supported on PEDOT:PSS is quantified. UV-vis spectroscopy is employed to quantify dimerization, time-resolved neutron reflectivity to resolve the vertical composition stratification, and atomic force microscopy for demixing and coarsening in thin films. At the conventional thermal stress test temperature of 85 °C (and even up to the PS glass transition), photodimerization dominates, resulting in relative morphological stability. Prior illumination is found to result in improved stability upon high temperature annealing, compatible with the need for dedimerization to occur prior to structural relaxation. Modeling of the PCBM surface segregation data suggests that only PCBM monomers are able to diffuse and that illumination provides an effective means to control dimer population, and thus immobile fullerene fraction, in the timescales probed. The results provide a framework for understanding of the stability of organic solar cells under operating conditions.

1. Introduction

The fulfillment of the potential of organic solar cells (OSC) requires both efficiency and long term stability to be improved.^[1] With current record power conversion efficiency (PCE) for a single junction bulk heterojunction OSC over 11.5%, and expected to continue to increase with the development of new donor polymer materials,^[2,3] this technology remains competitive. Under operation solar cells are exposed to a range of environmental stresses, including exposure to oxygen and humidity, and thermal and light fluctuations, resulting in several performance loss mechanisms.^[4–6] While efficient encapsulation can mitigate some factors, exposure to light and heat are intrinsic to solar cell operation and thus remain the focus of considerable research.^[7–9]

Morphological changes within the active layer of a bulk heterojunction, for instance via crystallization, or demixing and coarsening of the donor/acceptor blend, can evidently result in performance loss (as well as improvement),^[10–12] However, the initial light exposure of OSCs often results in “burn-in,” manifested by an initial exponential loss of device efficiency.^[13,14] The exact mechanism however has remained elusive, but correlations with a number of factors including polymer crystallinity,^[15,16] spinodal demixing,^[17] fullerene and polymer crosslinking,^[18] reactions with device contacts,^[19] and fullerene dimerization^[20,21] have been proposed.


The photopolymerization of fullerenes was first reported by Eklund and co-workers over 20 years ago,^[22–24] and found to proceed by a 2+2 cycloaddition. The reaction mechanism in C₆₀ requires the alignment between one of 30 double bonds from two molecules separated by less than 4.2 Å,^[23] under well-defined topo-chemical conditions. Photogenerated states required to initiate the cycloaddition are formed upon absorption at all wavelengths above the band edge with the reaction rate per photon shown to be independent of intensity.^[22,25] This C₆₀ polymerization reaction can be thermally reversed and the activation energy for decomposition was estimated to be ≈1.25 eV.^[26] Certain fullerene derivatives, including phenyl-C61-butyric acid methyl ester (PC₆₀BM) but not PC₇₀BM, undergo an analogous process although, due to steric hindrance, generally

S. Pont, Prof. J. R. Durrant, Prof. J. T. Cabral
Centre for Plastic Electronics
Imperial College London
London SW7 2AZ, UK
E-mail: j.cabral@imperial.ac.uk

S. Pont, Prof. J. R. Durrant
Department of Chemistry
Imperial College London
London SW7 2AZ, UK

Dr. F. Foglia,^[†] Prof. J. T. Cabral
Department of Chemical Engineering
Imperial College London
London SW7 2AZ, UK

Prof. A. M. Higgins
College of Engineering
Swansea University
Bay Campus, Swansea SA1 8EN, UK

 The ORCID identification number(s) for the author(s) of this article can be found under <https://doi.org/10.1002/adfm.201802520>.

^[†]Present address: Institute of Pharmaceutical Science, King's College London, Waterloo, London SE1 9NH, UK

© 2018 The Authors. Published by WILEY-VCH Verlag GmbH & Co. KGaA, Weinheim. This is an open access article under the terms of the Creative Commons Attribution License, which permits use, distribution and reproduction in any medium, provided the original work is properly cited.

The copyright line of this paper was changed on 18 September 2018 after initial publication.

DOI: 10.1002/adfm.201802520

form dimers (and possibly trimers) rather than polymeric chains.^[27,28] Edman and co-workers^[29,30] investigated the mechanism for neat phenyl-C61-butyric acid methyl ester (PCBM) exposed to UV light of varying intensity, highlighting the importance of triplet state formation to rationalize phototransformation kinetics. Upon blending of fullerenes and derivatives with polymers, this rich photochemistry is largely preserved, and the diffusion and association kinetics, as well as percolation conditions are believed to be mediated by the polymer matrix. Wong et al.^[31] reported the selective photopatterning of polystyrene/C₆₀ thin films and their improved morphological stability upon exposure to trivial visible light doses. PCBM dimerization in solar cells was also found to improve morphological stability^[28,32,33] and increase lifetime, as measured by the loss of performance (PCE) over time.^[28,32] This stabilization effect was also observed upon addition of chemically (rather than photochemically) synthesized fullerene dimers,^[34] which is likely related to the combined frustration of the fullerene crystallization processes and their reduced mobility. Substrate segregation^[35] and deposition methods,^[36] combined with light exposure, were found to synergistically prolong the lifetime of PCDTBT:PC₆₀BM in excess of 200 times, compared to a reference device. However, other reports suggest detrimental^[20,21] or neutral^[37] effects to PCE upon illumination. In the former, PCBM dimerization has been proposed to degrade PCE due to reduced charge carrier mobility, while in the latter the degradation mechanism has been associated instead to the accumulation of free radicals in the active layer. Further, while a range of systems exhibit performance loss over time, the fundamental nature of the process appears to be system-dependent and involving both the active layer and interfaces (compared systematically for P3HT and PCDTBT blends^[19]). Evidently, a range of failure processes are likely responsible for the diverse “burn-in” and “stabilization” observations, and further work in this area is needed.

In particular, the practical utilization of solar cells involves the simultaneous exposure to varying temperature and light intensity over time, with diurnal and seasonal fluctuations, and these effects are adversarial and competitive, at least in what concerns fullerene phototransformations. With these ideas in mind, we examine the interplay between PCBM photo-induced dimerization and thermally induced decomposition to assess their overall impact on the morphological stability of a polymer:fullerene blend. To our knowledge, this is the first in-operando investigation coupling thermal and light stresses on PCBM:polymer thin films.

2. Results and Discussion

Given the complexities discussed in the previous section, we select a model system of PCBM and an amorphous non-conjugated polymer, polystyrene (PS), in order to resolve the physical–chemical changes of PCBM alone. The active layer is deposited on poly(3,4-ethylenedioxythiophene):polystyrene sulfonate (PEDOT:PSS) to ensure representative bottom interface properties of standard devices. The sample architecture is thus Si/PEDOT:PSS/PS:PCBM where PCBM concentration was varied from 20% to 80%. **Figure 1a** illustrates the experimental plan, which investigates the separate and combined effects of light exposure and thermal exposure.

Two thermal profiles were examined: i) “isothermal” conditions at 85 °C, corresponding to usual thermal stress tests, for 10 h, followed by annealing at 120 °C, and a ii) “thermal ramp” from 20 to 100 °C, approaching the glass transition temperature, T_g , of the PS matrix. These are illustrated in the middle panels of Figures 1b,c. Each profile was examined both under “dark” and “illumination” conditions (1 Sun equivalent, white light), depicted in the bottom panels. UV–vis spectroscopy was employed to estimate the PCBM dimer:monomer population, using a previously reported absorbance feature at 320 nm.^[27]

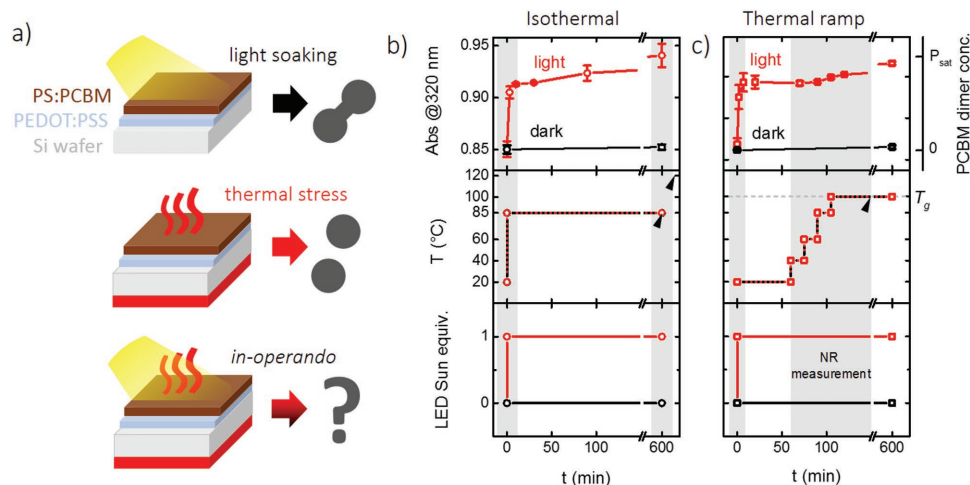


Figure 1. a) Schematic of PCBM photodimerization and thermal decomposition processes in a supported thin film, as well as simultaneous exposure to light and thermal stress following a time-varying profile, relevant for the practical use of solar cells. Conditions of b) isothermal stress and c) thermal ramping, with (red) and without (black) illumination. The top panels show the PCBM dimer concentration estimated by UV–vis spectroscopy (shown here for a 0.65:0.35 PS:PCBM sample); the middle and bottom panels show the temperature and illumination profiles (1 Sun equivalent). Shaded areas correspond to conditions of neutron reflectivity (NR) measurements and markers (►) indicate points of AFM measurements. All samples used in this study have the architecture Si/PEDOT:PSS/PS:PCBM and varying blend ratios, with $\phi(\text{PCBM}) = 0.2, 0.35, 0.5, 0.65, 0.8$ mass fraction.

Populations for the four conditions studied are given in the top panel of Figure 1b,c, shown here for a 0.65:0.35 PS:PCBM blend. Under these conditions, the PCBM dimer concentration was found to approach saturation within 30 min of illumination, while under dark (control) conditions PCBM remains in monomer form. Representative UV-vis absorbance data are provided in Figure S2 (Supporting Information).

A combination of atomic force microscopy (AFM) and neutron reflectivity (NR) was employed to, respectively, resolve in-plane morphological changes and component stratification normal to the surface. From 20% to 80% PCBM there is a large variation in blend morphology (Figure S3, Supporting Information), reminiscent of nucleation at low PCBM loading, to spinodal decomposition at 80% PCBM, accompanied by an increase of pattern amplitude. Neutron reflectivity (Figures S7 and S5, Supporting Information) reveals that the PCBM composition is broadly uniform throughout the film, and consistent with precursor concentrations. Both measurements show that after 10 h of thermal stress at 85 °C, PS:PCBM film morphology remains largely unchanged at all compositions, regardless of illumination.

This result is not unexpected as 85 °C is below the glass transition temperature of the polymer matrix ($T_g(\text{PS}) \approx 100$ °C),

which is not expected to be significantly affected by addition of fullerenes.^[38,39] While photoexcitations with energy greater than the bandgap can relax to the band edge, potentially releasing excess energy as a phonon, and in turn cause local temperature hot spots, such photo-induced local heating effects, if present, are modest and do not result in morphological instability, even in the vicinity of $T_g(\text{PS})$. Even though photochemical changes are evidently taking place under illumination, as shown in Figure 1b, these do not impact morphology, either in terms of topography or vertical stratification, since the glassy polymer matrix restricts fullerene mobility at this relatively modest, but standard thermal stress condition.

We next consider the effect of thermal stress above the T_g of the polymer matrix, namely at 120 °C in the dark, following prior light exposure (10 h, 1 Sun equivalent) or a dark control. AFM measurements were acquired at various time intervals, as shown in Figure 2a for 20:80 PS:PCBM blends. Insets show the 2D Fourier transforms of the AFM images, from which a characteristic spinodal lengthscale can be extracted from the position of the maximum intensity of the spinodal ring (as shown in Figure S4 of the Supporting Information). Films not previously illuminated, shown in the top panel in Figure 2a, exhibit rapid coarsening of the spinodal

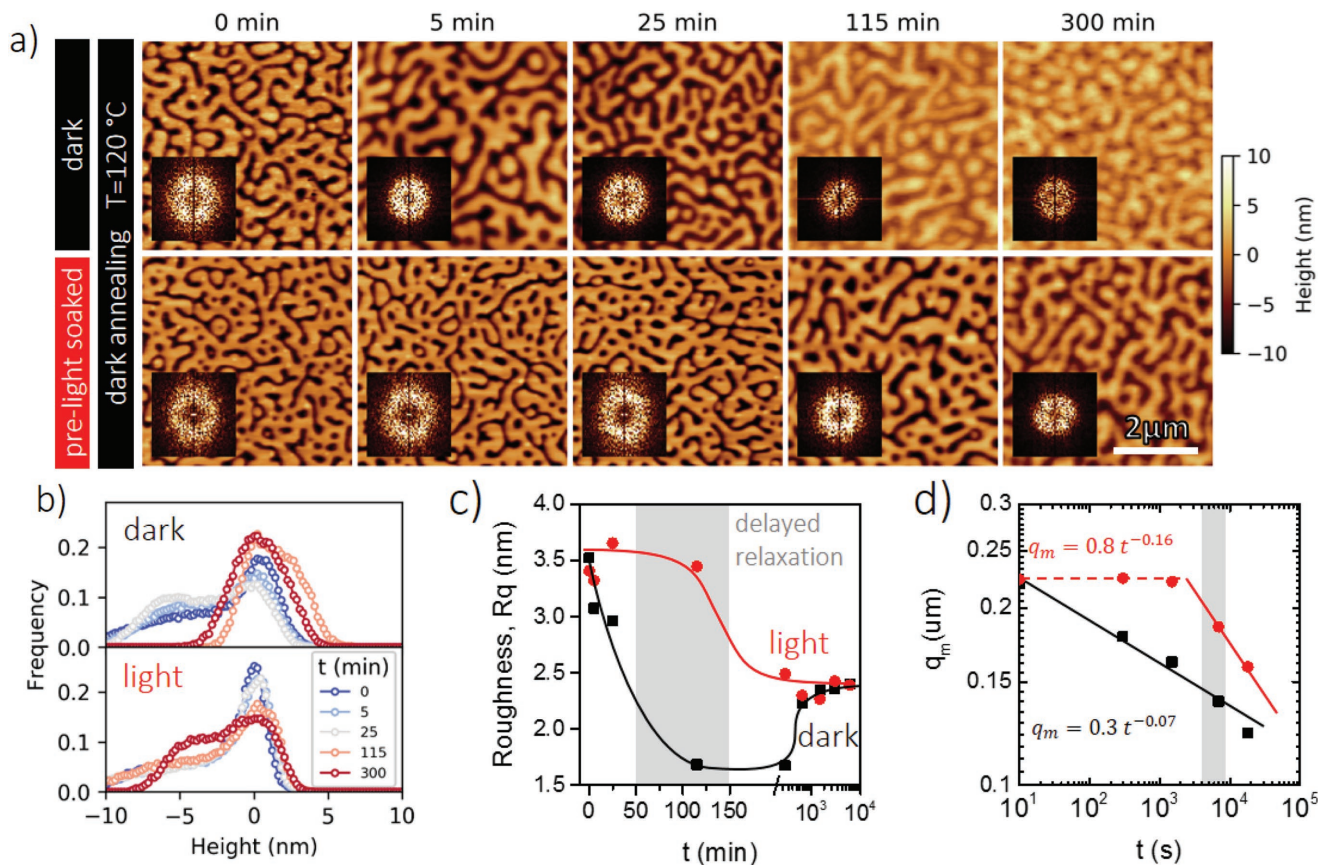


Figure 2. a) AFM images of 20:80 PS:PCBM blends annealed at 120 °C ($>T_g(\text{PS})$), in the dark, following 85 °C stress for 10 h, with and without prior light soaking (profile shown in Figure 1b). Insets are 2D Fourier transforms. b) Corresponding AFM height histogram and c) root mean squared (RMS) roughness. d) Peak position of the Fourier transform, q_m (computed as shown in Figure S4 of the Supporting Information), showing a delayed structural relaxation of the blend with prior light exposure. The shaded areas in (c) and (d) indicate the relaxation onset, interpreted as the time required for sufficient dimer decomposition to enable morphological coarsening.

structure and their topography relaxes, manifested by a decrease in image contrast. By comparison, morphology coarsening of prelight soaked films is effectively delayed (by ≈ 60 min). For the preilluminated sample, the AFM height histogram after 300 min (Figure 2b) is approximately equivalent to that of the dark sample after only 25 min annealing at 120 °C. The AFM root mean square (RMS) roughness, compared in Figure 2c, shows that the preilluminated film relaxes over much longer timescales than the dark sample. From a morphological perspective, coarsening appears to take place via a hydrodynamic relaxation process. The radially averaged 2D Fourier transforms of the AFM height data, Figure 2d, show that preilluminated samples exhibit a time-invariant plateau, before coarsening commences. The corresponding peak wavenumber q_m follows a power law time-dependence, as expected; however the power is much less than 1 which is expected under thin-film confinement.^[40] This lag time is interpreted as due to the time required for thermal decomposition (or “dedimerization”) of PCBM to occur, thus enabling sufficient mobility required for the coarsening of the spinodal structure. The timescale agrees with previous data that shows that after 60 min annealing at 120 °C the dimer concentration reduces by $\approx 50\%$.^[28] These results show that, at temperatures greater than matrix T_g , the presence of dimers inhibits the relaxation of the spinodal morphology, and

significant decomposition must occur before the mechanism can initiate. Dimerisation has thus a stabilization effect on the morphology which is visible at these thermal stresses.

To examine the evolution of the cross-sectional composition profiles as a function of temperature, NR measurements of representative films were acquired from room temperature up to T_g (Figures S7 and S8, Supporting Information). No significant changes in PCBM cross-sectional distribution occur until T_g is reached beyond which, after 30 min annealing at 100 °C a rapid enrichment of PCBM is observed at the PEDOT:PSS interface, quantified below. This is observed at all blend ratios (Figure S9, Supporting Information), except at 80% PCBM likely due to its lower matrix mobility. The enrichment layer is $\approx 20\text{--}30$ Å deep, corresponding to 1–3 fullerene units^[41] coating the PEDOT:PSS surface, and the maximum SLD of this layer approaches that of neat PCBM.

Following the thermal ramp from room temperature to 100 °C, AFM data compare the topographical stability of all blend compositions exposed to thermal stress with and without illumination, in Figure 3a. Qualitatively, a lower contrast can be seen in the dark samples, further quantified in Figure 3b, which show narrower height distributions compared to the illuminated films. The latter are similar to films annealed at 85 °C for 10 h, demonstrating that light exposure has effectively imparted morphological stability. The

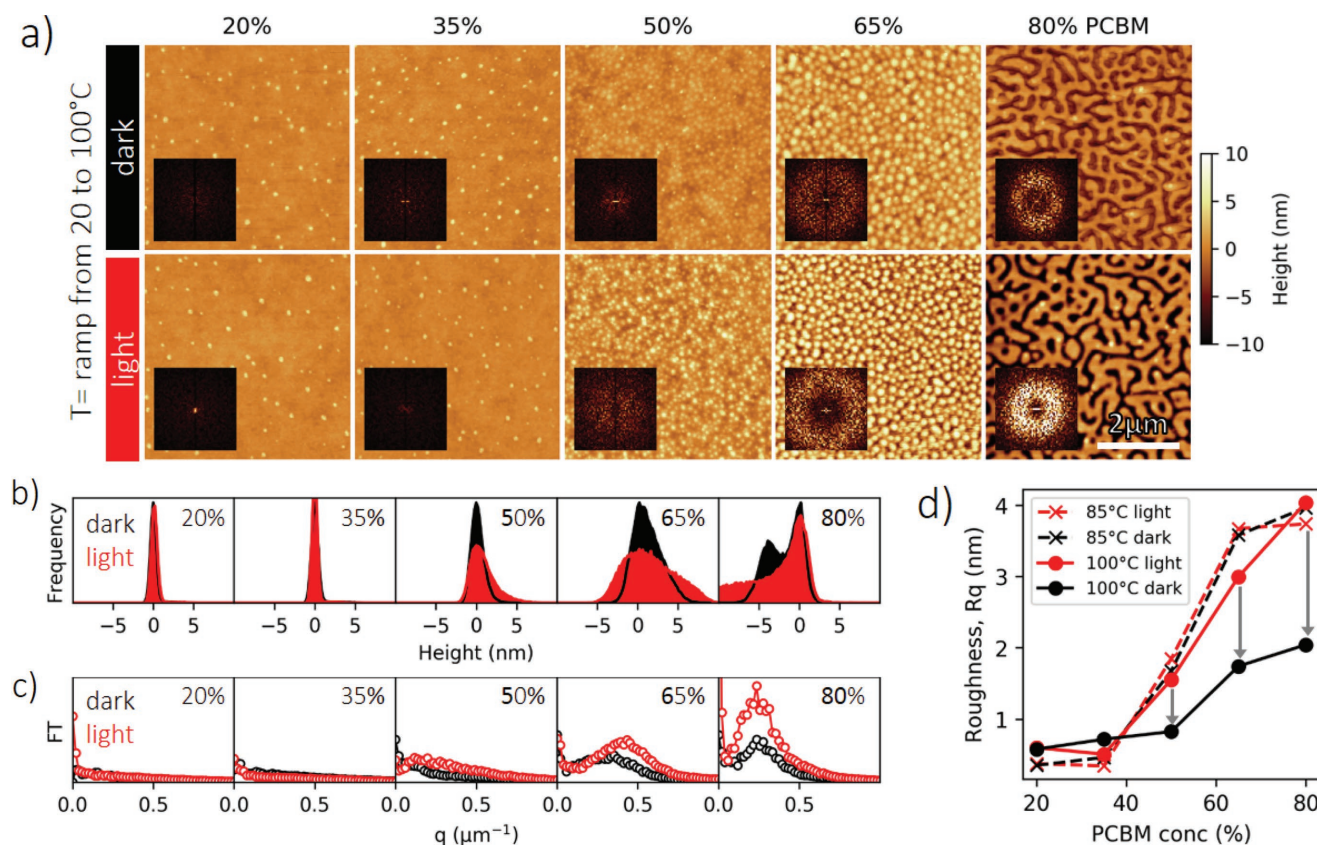


Figure 3. a) AFM images following thermal ramping from room temperature to 100 °C (depicted in Figure 1c) for PS:PCBM blends of all compositions investigated, showing characteristic nucleation and spinodal morphologies. Significant relaxation of the topography is seen for the blends annealed in the dark, shown by a reduction in contrast of the AFM images and narrowing of the b) height histograms. c) Radial average of the 2D Fourier transforms shown in the insets of (a). d) Corresponding RMS roughness and comparison with isothermal data (85 °C, 10 h), showing the enhanced morphological stability of illuminated samples by contrast with blends annealing in the dark, for $T \geq T_g$ (PS).

relaxation of the topography corroborates the observations of in situ NR data (Figure S9, Supporting Information). The 2D Fourier transforms, shown in Figure 3c, indicate that the periodicity of the structure is not significantly affected by these parameters, except for a modest peak shift toward lower q for dark samples of intermediate compositions, which is expected upon coarsening. The RMS roughness estimates in Figure 3d provide arguably the clearest observation of this point: data for samples illuminated and thermally stressed at 100 °C (for 30 min) superpose with low temperature data, with or without illumination, and are morphologically “stable” (up to this time and temperature), while dark samples thermally stressed at 100 °C are unstable.

In order to quantify the interplay between dimer formation and morphological instability under light and thermal stress, time-resolved NR measurements of PS:PCBM films were carried out during thermal annealing at 100 °C ($\approx T_g(\text{PS})$) with and without simultaneous illumination (1 Sun equivalent). Representative NR data (and fits) for 50:50 PS:PCBM (a,b) without and (c,d) with light exposure are shown in Figure 4. The solid lines are batch fits to the data, computed following the procedure detailed in the experimental section. On top of the 12 Å silicon oxide layer, the PEDOT:PSS layer thickness ranged from 295 to 305 Å, with a scattering length density (SLD) of $1.61 \times 10^{-6} \text{ \AA}^{-2}$. The SLD profiles quantify the kinetics of PCBM enrichment at the PEDOT:PSS (bottom) interface, which is

much greater for ‘dark’ than ‘light’ conditions. In fact, for the dark samples, the PCBM concentration at the PEDOT:PSS interface saturates at the SLD value of neat PCBM. In solar cell operation, the aggregation of electron-accepting PCBM toward the hole-transporting interface is generally detrimental to device performance, hampering the required extraction of electrons to the top contact and increasing recombination at the hole extracting interface. The symmetry and magnitude of component segregation is, however, known to be both interface- and polymer- dependent.

PCBM segregation kinetics were quantified by fitting the SLD over time at a fixed distance of 25 Å from the PEDOT:PSS interface, from which the PCBM concentration was estimated. Other criteria (e.g., peak integration) yielded similar results, and this procedure was repeated for all test conditions. Experimental results for 50:50 PS:PCBM are shown in Figure 4e: the PCBM concentration increases asymptotically over time, and can be empirically described by an (inverse) exponential relationship $\phi_{\text{interface}} = \phi_0 + (\phi_{\infty} - \phi_0)(1 - e^{-kt})$.

While it is clear that the presence of PCBM dimers improves the morphological stability of polymer:PCBM blends, the dimer population is governed by a subtle competition between light exposure and thermally induced decomposition. The latter can be described by an activated process with $E_A \approx 1 \text{ eV}$ ^[28] (similar to that of neat C₆₀^[26]) and becomes significant above

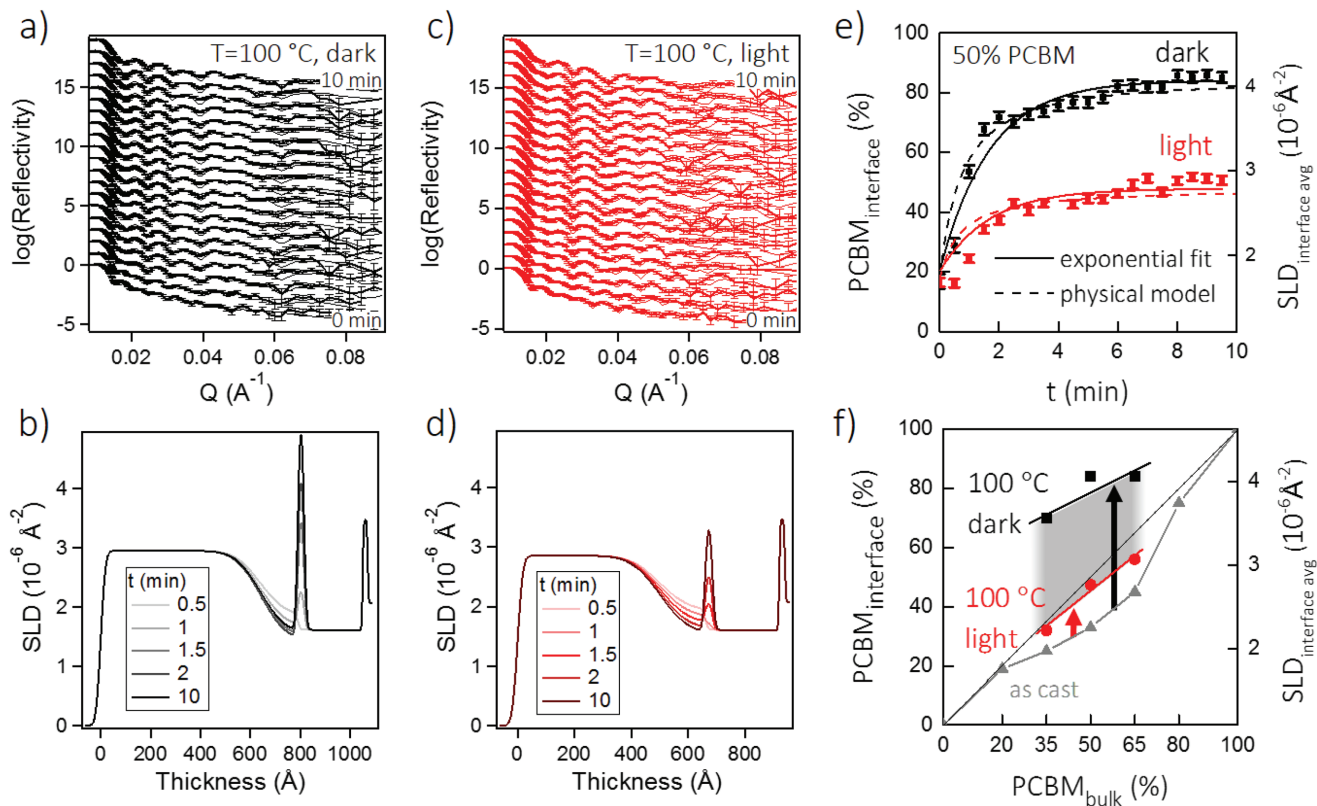


Figure 4. a) Time-resolved neutron reflectivity (NR) of 50:50 PS:PCBM blends annealed at 100 °C for 10 min with 30 s resolution. Solid lines are batch data fits. b) Corresponding scattering length density (SLD) profile, showing the PCBM enrichment at the PEDOT:PSS (bottom) interface. c,d) NR data and SLD for the same blend with simultaneous light exposure (1 Sun equivalent). e) Evolution of PCBM concentration (computed from SLD, shown on the right axis) at the bottom interface in both dark and light cases, with data fits (detailed in the text). f) Initial and final (asymptotic) PCBM concentration at the bottom interface, with and without light exposure; the diagonal gray line indicates the average PCBM composition in the film.

≈100 °C. This means that at lower temperatures (<100 °C), the forward (dimerization) reaction prevails under illumination conditions. The dimerization reaction (since it is a photochemical process) is likely to have a weak temperature dependence, associated with network diffusion and the statistics of topo-chemical requirements, although this must still be quantitatively examined. If so, at sufficiently high temperatures and competitive illumination, thermal decomposition can be expected to dominate. In our time-resolved NR measurements, we show that fullerene diffusion can take place even at simultaneous illumination and annealing at 100 °C, although the mobile (monomer) population is considerably reduced. Detailed modeling of these processes should enable the estimation of the dynamic dimer:monomer population and enable the prediction of morphological stability under in-operando conditions.

3. Conclusions

The morphological stability of polymer/fullerene solar cells to thermal stresses and light exposure was investigated with model PS:PCBM thin films. Our work builds upon numerous reports of C₆₀ and PCBM phototransformations, dimerization, and burn-in effects in organic solar cell stability, by our group and several others.^[20,21,28,32,33,36,42] To the best of our knowledge, however, this is the first time that the coupling of illumination, known to induce fullerene dimerization, and thermal stress, known to induce decomposition (or dedimerization), were simultaneously investigated. Examination of this coupling is essential for the understanding of morphological (and performance) stability of organic solar cells, which are exposed to modulated light and heat profiles with diurnal and seasonal variations during operation. The use of PS as a polymer matrix instead of a conjugated polymer (e.g., P3HT, PCDTBT) enabled us to clearly isolate the phototransformations in PCBM.

We do not observe significant morphological changes with this system upon annealing up to 100 °C (above the usual 85 °C thermal stress condition), regardless of light exposure, both in terms of topography (measured by AFM) or component stratification (measured by NR). Above T_g , in the absence of light, we observe a gradual relaxation of the thin film topography and structural coarsening, which are significantly hindered for the light-exposed samples. Structural relaxation is effectively delayed in samples that have been previously exposed to light, compatible with the requirement of thermal de-dimerization occurring prior to relaxation. Employing NR, we observe no stratification up to 100 °C (i.e., up to T_g of the polymer matrix), beyond which PCBM rapidly enriches at the PEDOT:PSS interface. While thermally driven dedimerization has been established to occur above ≈80 °C (in the absence of light^[43]), we observe a significant dimer population under conditions of simultaneous light exposure and heat, up to 85–100 °C, even at long times. These results show that dimerization prevails under these competitive conditions, while the mobile monomer fraction remains able to diffuse.

We employ a temperature ramp to emulate the effect of temperature fluctuations in operation conditions and find that simultaneous light exposure effectively suppresses structural

relaxation at the top film interface, while film stratification is diminished. The kinetics of PCBM attraction to the bottom (PEDOT) interface were quantified by time-resolved NR and described by a simple model. Interestingly, we find the rate constant to be unchanged between illuminated and nonilluminated films; by contrast, the mobile PCBM population is significantly reduced upon illumination. These results are compatible with an interpretation of the dimer population being effectively immobile within these timescales and responsible for the hindered structural rearrangement processed observed. Our findings are relevant to the understanding of stability in polymer:fullerene cells under operating conditions, that involve simultaneous (and varying) light and thermal stress exposure, and provide a fundamental and quantitative framework for morphological control.

4. Experimental Section

Sample Preparation: Solutions of phenyl-C61-butyric acid methyl ester, PCBM, (supplied by Nano-c) and polystyrene, PS, with $M_w = 100 \text{ kg mol}^{-1}$ (supplied by BDH Chemicals LTD) were prepared at a combined concentration of 25 mg mL^{-1} in chlorobenzene. Neutron reflectivity samples were prepared on silicon wafer substrates with a diameter of 50 mm and UV-vis absorption samples were prepared on glass. Substrates were plasma treated in an oxygen atmosphere with a Emitech K1050X before PEDOT:PSS (Al 4083) was spun at 1000 rpm for 40 s. Stock solutions of PS (25 mg/mL) and PCBM (25 mg/mL) were mixed up at volumetric ratios of 20:80, 35:65, 50:50, 65:35, and 80:20 and spin coated at 1500 rpm for 30 s, to give thin films with equivalent mass ratios. The resulting film thicknesses ranged from 90 to 120 nm, measured by stylus profilometry (Dektak XT) and confirmed by NR. Samples are found to be uniform and of consistent thickness across the NR sampling area (Figure S1, Supporting Information).

Illumination and Annealing: It was carried out in a nitrogen filled glovebox with oxygen and humidity levels kept <15 ppm. A Bridgelux 4000 K white LED light source was used with the spectrum shown in Figure S2 (Supporting Information). The intensity was matched to give equivalent photocurrent response from of a silicon photodiode at AM1.5G. The rates of dimerisation under the LED irradiance and under AM1.5G were found to be comparable (Figure S2, Supporting Information), thus validating the use of the former for in situ NR experiments. Thermal annealing was carried out on a hotplate, calibrated in-situ with and without illumination.

UV-Vis Absorption Spectroscopy: It was carried out with a Shimadzu UV-1601 spectrophotometer with measurements taken from 300 to 350 nm in transmission mode. To determine an assay of PCBM dimer concentration the absorbance was normalized to a peak at ≈340 nm and the change at the peak minimum at ≈320 nm monitored.

Atomic Force Microscopy: It was carried out with a Bruker Innova microscope in tapping mode at 0.2 Hz with Si tips (MPP-11100-W, Bruker) to evaluate blend morphology and dependence on annealing temperature, time, and light exposure. Data analysis of the topography data extracted the height frequency distribution (from the “numpy histogram” function), Fourier transform (from with “scipy fftpack fft2” function), and surface roughness, R_q , using custom code written in Python 3.0 (provided in Supporting Information).

Neutron Reflectivity: The measurements were carried out at the D17 reflectometer at the Institut Laue Langevin (Grenoble, France). Both static and time-resolved measurements were employed to determine the cross-sectional structure of PS/PCBM films exposed to various environmental conditions. Static measurements were performed at angles 0.9° and 3.4°, covering a momentum transfer normal to the surface ($Q = (4\pi/\lambda)\sin\theta$) ranging from 0.006 to 0.3 \AA^{-1} . Kinetic measurements were acquired at a single angle of 1°, yielding $0.01 \leq Q \leq 0.09 \text{ \AA}^{-1}$, with 30 s time resolution, employing an enclosed hot stage

with a steady N₂ gas purge, and an Bridgelux 4000 K white LED light source; the temperature was controlled directly at the measured sample and any offset accounted for. Specular reflectivity profiles were analyzed using Motofit,^[44] both in single and batch fit mode for the static and kinetic measurements, respectively, enabling simultaneous, self-consistent data fitting. The batch fit function in Motofit was used to fit the kinetic data with a number of constraints that we found to improve the robustness of the data fit. The initial fit at $t = 0$ min was obtained from the full- q measurements shown in the Figure S9 (Supporting Information). Subsequently, the roughness and thickness were fixed, as well as the SLD values, except for two: that of a 30 Å layer at the bottom interface, and that of an adjacent layer of 150 Å toward the bulk of the film. A genetic + Levenberg–Marquardt algorithm was used to optimize the fit to the data. The uncertainty from the algorithmic fit is shown in the error bars of Figure 4e of the main paper. A detailed example of the fitting procedure, sensitivity of the fit to SLD changes, and uncertainty estimation is shown in Figure S6 (Supporting Information).

Appendix: Diffusive Modeling of PCBM Surface Enrichment

A simple coarse-grained model, combining diffusion and surface attraction, can describe the full cross-sectional composition profile of PCBM, including the enrichment of PCBM at the PEDOT:PSS interface. We write the PCBM flux as a sum of two components, a Fickian diffusion term and an additional flux driven by the attractive surface field, taken as an attractive exponential (although a high powerlaw yields similar agreement with data). This is parameterized as

$$J(x, t) = -D \frac{\partial \phi(x, t)}{\partial x} + \beta (\phi_{\infty} - \phi(x, t)) \exp(-x/\gamma) \quad (1)$$

where $\phi(x, t)$ is the PCBM concentration, x is the distance from the PEDOT:PSS interface, t is time, D is an effective diffusion coefficient of PCBM within the matrix, β and γ are the depth and range of the attractive potential well; as before ϕ_{∞} is the saturation concentration of PCBM at the interface. From the initially measured composition profile $\phi(x, t = 0)$, this solution was iteratively evolved over time until a steady state solution was reached. We find that a single diffusion coefficient $D \approx 5 \times 10^{-9} \text{ cm}^2 \text{ s}^{-1}$ satisfactorily describes all datasets, in line with the single k parameter found with the descriptive fit. This D value is of the same order of magnitude, albeit larger, than previously reported values for PCBM within various polymer matrices ($0.3\text{--}1.3 \times 10^{-9} \text{ cm}^2 \text{ s}^{-1}$) at these temperatures.^[45,46] Similarly, we find that a single $\beta \approx 0.09 \text{ cm s}^{-1}$ and $\gamma \approx 18 \text{ Å}$ accounts for the attractive surface potential (from PEDOT:PSS), which seems sensible since the interface remains the same for all blend compositions and light exposure conditions. The asymptotic PCBM surface composition differs in every case, as expected, as we find $\phi_{\infty} = 0.50$ and 0.85 , respectively, for the 50:50 PS:PCBM films annealed at 100 °C with and without illumination. The agreement with the spatiotemporal PCBM composition data is very good, as shown in Figure S12 (Supporting Information), despite the simplicity of the model. The agreement with the interfacial PCBM composition, shown as dashed lines in Figure 4e is equally very good.

Supporting Information

Supporting Information is available from the Wiley Online Library or from the author.

Acknowledgements

The authors thank the Engineering and Physical Sciences Research Council (EPSRC, UK, EP/L016702/1) and Solvay for financial support, and the Institut Laue Langevin (ILL, Grenoble) for beamtime. The authors are grateful to Philipp Gutfreund for assistance during neutron reflectivity measurements and Jack Douglas (NIST) for discussions on modeling fullerene segregation. Data presented in this paper are available on the Zenodo repository at 10.5281/zenodo.1300949.

Conflict of Interest

The authors declare no conflict of interest.

Keywords

fullerenes, photochemistry, photovoltaic devices, polymeric materials, solar cells

Received: April 13, 2018

Revised: June 29, 2018

Published online: August 13, 2018

- [1] S. A. Gevorgyan, M. V. Madsen, B. Roth, M. Corazza, M. Hösel, R. R. Søndergaard, M. Jørgensen, F. C. Krebs, *Adv. Energy Mater.* **2016**, *6*, 1501208.
- [2] J. Zhao, Y. Li, G. Yang, K. Jiang, H. Lin, H. Ade, W. Ma, H. Yan, *Nat. Energy* **2016**, *1*, 15027.
- [3] S. Zhang, L. Ye, J. Hou, *Adv. Energy Mater.* **2016**, *6*, 1.
- [4] H. K. H. Lee, A. M. Telford, J. A. Röhr, M. F. Wyatt, B. Rice, J. Wu, A. de Castro Maciel, S. M. Tuladhar, E. Speller, J. McGettrick, J. R. Searle, S. Pont, T. Watson, T. Kirchartz, J. R. Durrant, W. C. Tsoi, J. Nelson, Z. Li, *Energy Environ. Sci.* **2018**, *11*, 417.
- [5] W. R. Mateker, M. D. McGehee, *Adv. Mater.* **2017**, *29*, 1603940.
- [6] I. Fraga Domínguez, A. Distler, L. Lüer, *Adv. Energy Mater.* **2017**, *7*, 1601320.
- [7] M. Jørgensen, K. Norrman, S. A. Gevorgyan, T. Tromholt, B. Andreasen, F. C. Krebs, *Adv. Mater.* **2012**, *24*, 580.
- [8] S. Savagatrup, A. D. Printz, T. F. O'Connor, A. V. Zaretski, D. Rodriguez, E. J. Sawyer, K. M. Rajan, R. I. Acosta, S. E. Root, D. J. Lipomi, *Energy Environ. Sci.* **2015**, *8*, 55.
- [9] P. Cheng, X. Zhan, *Chem. Soc. Rev.* **2016**, *45*, 2544.
- [10] W. Ma, C. Yang, A. J. Heeger, *Adv. Mater.* **2007**, *19*, 1387.
- [11] S. H. Park, A. Roy, S. Beaupré, S. Cho, N. Coates, J. S. Moon, D. Moses, M. Leclerc, K. Lee, A. J. Heeger, *Nat. Photonics* **2009**, *3*, 297.
- [12] A. J. Heeger, *Adv. Mater.* **2014**, *26*, 10.
- [13] T. M. Clarke, C. Lungenschmied, J. Peet, N. Drolet, K. Sunahara, A. Furube, A. J. Mozer, *Adv. Energy Mater.* **2013**, *3*, 1473.
- [14] W. R. Mateker, I. T. Sachs-Quintana, G. F. Burkhard, R. Cheacharoen, M. D. McGehee, *Chem. Mater.* **2015**, *27*, 404.
- [15] T. Heumueller, T. M. Burke, W. R. Mateker, I. T. Sachs-Quintana, K. Vandewal, C. J. Brabec, M. D. McGehee, *Adv. Energy Mater.* **2015**, *5*, 1500111.
- [16] T. Heumueller, W. R. Mateker, I. T. Sachs-Quintana, K. Vandewal, J. a. Bartelt, T. M. Burke, T. Ameri, C. J. Brabec, M. D. McGehee, *Energy Environ. Sci.* **2014**, *7*, 2974.

- [17] N. Li, J. D. Perea, T. Kassar, M. Richter, T. Heumueller, G. J. Matt, Y. Hou, N. S. Güldal, H. Chen, S. Chen, S. Langner, M. Berlinghof, T. Unruh, C. J. Brabec, *Nat. Commun.* **2017**, *8*, 14541.
- [18] A. Tournebize, A. Rivaton, J.-L. Gardette, C. Lombard, B. Pépin-Donat, S. Beaupré, M. Leclerc, *Adv. Energy Mater.* **2014**, *4*, 1301530.
- [19] E. Voroshazi, I. Cardinaletti, T. Conard, B. P. Rand, *Adv. Energy Mater.* **2014**, *4*, 1400848.
- [20] A. Distler, T. Sauermann, H.-J. Egelhaaf, S. Rodman, D. Waller, K.-S. Cheon, M. Lee, D. M. Guldi, *Adv. Energy Mater.* **2014**, *4*, 1300693.
- [21] T. Heumueller, W. R. Mateker, A. Distler, U. F. Fritze, R. Checharoen, W. H. Nguyen, M. Biele, M. Salvador, M. von Delius, H.-J. Egelhaaf, M. D. McGehee, C. J. Brabec, *Energy Environ. Sci.* **2016**, *9*, 247.
- [22] Y. Wang, J. Holden, Z.-H. Dong, X.-X. Bi, P. Eklund, *Chem. Phys. Lett.* **1993**, *211*, 341.
- [23] P. Zhou, Z.-H. Dong, A. Rao, P. Eklund, *Chem. Phys. Lett.* **1993**, *211*, 337.
- [24] A. M. Rao, P. Zhou, K.-A. Wang, G. T. Hager, J. M. Holden, Y. Wang, W. T. Lee, X.-X. Bi, P. C. Eklund, D. S. Cornett, M. A. Duncan, I. J. Amster, *Science* **1993**, *259*, 955.
- [25] A. Distler, *Ph.D. thesis*, University of Erlangen-Nuremberg **2015**.
- [26] Y. Wang, J. Holden, X.-x. Bi, P. Eklund, *Chem. Phys. Lett.* **1994**, *217*, 413.
- [27] A. Dzwilewski, T. Wägberg, L. Edman, *J. Am. Chem. Soc.* **2009**, *131*, 4006.
- [28] H. C. Wong, Z. Li, C. H. Tan, H. Zhong, Z. Huang, H. Bronstein, I. McCulloch, J. T. Cabral, J. R. Durrant, *ACS Nano* **2014**, *8*, 1297.
- [29] J. Wang, C. Larsen, T. Wägberg, L. Edman, *Adv. Funct. Mater.* **2011**, *21*, 3723.
- [30] J. Wang, J. Enevold, L. Edman, *Adv. Funct. Mater.* **2013**, *23*, 3220.
- [31] H. C. Wong, A. M. Higgins, A. R. Wildes, J. F. Douglas, J. T. Cabral, *Adv. Mater.* **2013**, *25*, 985.
- [32] Z. Li, H. C. Wong, Z. Huang, H. Zhong, C. H. Tan, W. C. Tsoi, J. S. Kim, J. R. Durrant, J. T. Cabral, *Nat. Commun.* **2013**, *4*, 1.
- [33] F. Piersimoni, G. Degutis, S. Bertho, K. Vandewal, D. Spoltore, T. Vangerven, J. Drijkoningen, M. K. Van Bael, A. Hardy, J. D'Haen, W. Maes, D. Vanderzande, M. Nesladek, J. Manca, *J. Polym. Sci., Part B: Polym. Phys.* **2013**, *51*, 1209.
- [34] B. C. Schroeder, Z. Li, M. A. Brady, G. C. Faria, R. S. Ashraf, C. J. Takacs, J. S. Cowart, D. T. Duong, K. H. Chiu, C.-H. Tan, J. T. Cabral, A. Salleo, M. L. Chabinyc, J. R. Durrant, I. McCulloch, *Angew. Chem., Int. Ed.* **2014**, *53*, 12870.
- [35] Z. Li, K. Ho Chiu, R. Shahid Ashraf, S. Fearn, R. Dattani, H. Cheng Wong, C.-H. Tan, J. Wu, J. T. Cabral, J. R. Durrant, *Sci. Rep.* **2015**, *5*, 15149.
- [36] C.-H. Tan, H. C. Wong, Z. Li, D. G. Bucknall, J. R. Durrant, J. T. Cabral, *J. Mater. Chem. C* **2015**, *3*, 9551.
- [37] L. N. Inasaridze, A. I. Shames, I. V. Martynov, B. Li, A. V. Mumyatov, D. K. Susarova, E. A. Katz, P. A. Troshin, *J. Mater. Chem. A* **2017**, *5*, 8044.
- [38] A. Sanz, H. C. Wong, A. J. Nedoma, J. F. Douglas, J. T. Cabral, *Polymer* **2015**, *68*, 47.
- [39] G. Bernardo, N. Deb, S. M. King, D. G. Bucknall, *J. Polym. Sci., Part B: Polym. Phys.* **2016**, *54*, 994.
- [40] H. C. Wong, J. T. Cabral, *Phys. Rev. Lett.* **2010**, *105*, 038301.
- [41] M. S. Dresselhaus, G. Dresselhaus, P. Eklund, *Science of Fullerenes and Carbon Nanotubes*, Academic Press, San Diego **1995**.
- [42] X. Li, M. Ibrahim Dar, C. Yi, J. Luo, M. Tschumi, S. M. Zakeeruddin, M. K. Nazeeruddin, H. Han, M. Grätzel, *Nat. Chem.* **2015**, *7*, 703.
- [43] N. Wang, X. Tong, Q. Burlingame, J. Yu, S. R. Forrest, *Solar Energy Mater. Solar Cells* **2014**, *125*, 170.
- [44] A. Nelson, *J. Appl. Crystallogr.* **2006**, *39*, 273.
- [45] G. A. Berriman, J. L. Holdsworth, X. Zhou, W. J. Belcher, P. C. Dastoor, *AIP Adv.* **2015**, *5*, 097220.
- [46] N. D. Treat, T. E. Mates, C. J. Hawker, E. J. Kramer, M. L. Chabinyc, *Macromolecules* **2013**, *46*, 1002.